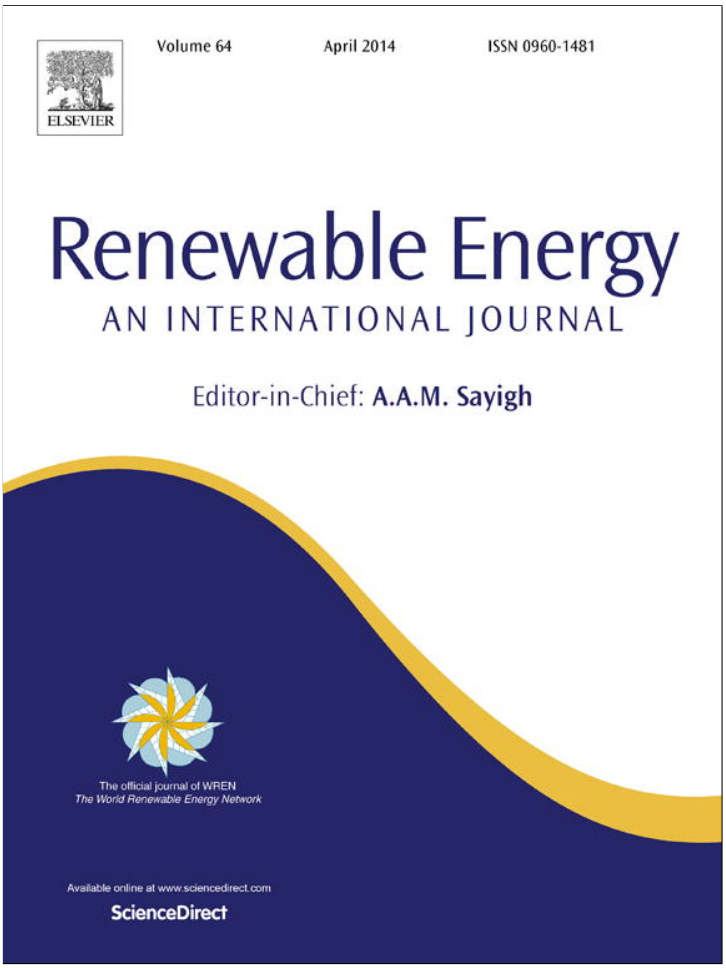

Renewable Energy 64 (2014) 306–313

Contents lists available at ScienceDirect

Renewable Energy

journal homepage: www.elsevier.com/locate/renene

Determining the infrared reflectance of specular surfaces by using thermographic analysis

Silvana Flores Larsen*, Marcos Hongn

Instituto de Investigaciones en Energía No Convencional (INENCO, UNSa – CONICET), Universidad Nacional de Salta, Av. Bolivia 5150, A4408FVY Salta, Argentina

ARTICLE INFO

Article history:
Received 8 March 2013
Accepted 13 November 2013
Available online 13 December 2013

Keywords:
Infrared reflectance
Thermography
Infrared optical properties
Specular materials

ABSTRACT

Specular surfaces as glass, mirrors and metals are commonly used in solar devices and in building facades. Determining the temperature distribution of such kind of surfaces allows estimating their thermal losses and detecting hot spots and temperature gradients that provokes material stress and rupture. In this sense, thermography is a non-contact measurement technique that is capable to quickly scan and record these surface temperature distributions, but when specular materials are inspected the infrared reflectance becomes a crucial parameter. This work describes a methodology to measure the reflectance of specular materials for different incidence angles in the infrared range 8 μm–14 μm, by using a thermographic camera and an infrared radiation source. The methodology includes the analysis of errors in the estimation of the reflectance and how to select the temperature of the source that minimizes these errors. The method is applied to different specular surfaces commonly used in building facades and solar devices, whose infrared specular reflectances are estimated for different incidence angles. The obtained results are analyzed in order to provide valuable information for in-situ thermographic measurements of specular surfaces.

1. Introduction

Specular surfaces as glass, mirrors and metals are commonly used in solar devices and in building facades. In solar devices they are used mostly as transparent covers (air and water solar heaters, heat pipes, solar absorber for linear Fresnel devices, photovoltaic modules, solar cookers, etc.) and as reflecting surfaces in solar concentrating devices (glass mirrors and aluminum sheets in Fresnel and CPC devices). In buildings, specular surfaces appear in windows, glazed and mirrored facades, glazing of Trombe walls, metallic facade covers, and so on. Determining the temperature distribution of such kind of surfaces allows to estimate their thermal losses, a very important parameter both, in building and solar applications, that influences the thermal performance and energy consumption of buildings and the efficiency in the case of solar devices (Albatici and Tonelli [1]). The knowledge of the surface temperature field also allows detecting hot spots and temperature gradients provoking material stress and rupture. Thermography is a non-contact measurement technique that is capable to quickly scan and record surface temperature distributions. A thermographic camera works by detecting the radiant energy, typically over a restricted range of wavelengths, emitted by the object of interest and by using Planck's radiation law to relate this energy to temperature. An optical system focuses the energy onto the detector, and a filter is used to select the appropriate wavelength range. This thermal energy is transformed into a visible image, where a color or a gray level is used to represent the point temperature. Nowadays, the application of thermography in buildings and solar devices is a usual qualitative diagnosis technique, but in quantitative applications the accuracy of the measurements depends on knowing the limitations and possible errors influencing the results. Thermography is an ideal measurement technique when the surfaces are inaccessible to other measure devices (as in the facades of high rise buildings), when surfaces receive high solar radiation levels that make unavailable the use of conventional contact sensors (as in the case of the absorbers of solar concentrators), for applications at urban level as when measuring heat island effects (Chudnovsky et al. [2]), to estimate the infrared reflectance of selective surfaces as the case of glasses treated to reflect a high portion of the infrared spectrum, etc. The quantitative infrared thermography in buildings is a very useful technique currently under development. Some valuable researches include the quantitative evaluation of thermal bridges in buildings (Asdrubali et al. [3]), who can estimate the thermal bridge effect as a percentage

* Corresponding author. Tel.: +54 387 4255578; fax: +54 387 4255489.
E-mail addresses: seflores@unsa.edu.ar, silvanafloreslarsen@gmail.com (S. Flores Larsen), marcoshongn@gmail.com (M. Hongn).

0960-1481/$ – see front matter © 2013 Elsevier Ltd. All rights reserved.
http://dx.doi.org/10.1016/j.renene.2013.11.049

Nomenclature

$e\%$	percentage relative error of the reflectance measurement (unitless)
$S_0(T)$	signal produced by the infrared sensor (V)
S_{sen}	electrical signal produced by sensor (V)
T_a	air temperature (°C)
T_r	apparent temperature of the source reflected on the target (°C)
T_s	source temperature (°C)
T_{surr}	surrounding temperature (°C)
T_t	target temperature (°C)
U	Overall heat transfer coefficient (W m^2 K^{-1})

Greek symbols

ε'	emittance set in the infrared camera when measuring the reflected image (unitless)
ε_λ	spectral emittance (unitless)
ε_t	target emittance in work camera range (unitless)
ε_s	source emittance in work camera range (unitless)
θ	incidence angle for infrared radiation (°)
λ	wavelength (μm)
ρ_t	target reflectance in work camera range (unitless)
σ	Stefan–Boltzman constant (5.6697 × 10^{-8} W m^2 K^{-4})
τ_a	air transmittance (unitless)
$\Delta\rho_t$	absolute error of the reflectance measurement (unitless)
ΔT_s	absolute error when measuring T_s (°C)
ΔT_r	absolute error when measuring T_r (°C)
ΔT_a	absolute error when measuring T_a (°C)

increase of the wall transmittance by measuring the air temperature and by analyzing the corresponding thermogram. Other studies deal with the quantitative determination of the overall heat transfer coefficient (U-value) of building envelopes through infrared thermography: Fokaides and Kalogirou [4] proposed a technique to estimate U by measuring the wall temperature with an infrared camera and they determined the U-value of typical building construction in Cyprus. Recently, Lehmann et al. [5] performed a quantitative analysis of the individual influence of different parameters on the thermal images of building facades and developed a procedure to evaluate these images considering the thermal characteristics of the building itself and the climatic history preceding the infrared thermography. Marinetti and Cesaratto [6] proposed a transient method for emissivity measurement, which is based on the spectral response of the IR sensor and does not require emissivity references and reflected temperature knowledge. The authors used an IR camera operating in the mid-wave band (3–5 μm). Results showed that for outdoor measurements, the influence of emissivity was stronger than in the indoor case.

The mentioned studies deal with diffusing targets. The application of infrared thermography for specular targets is complex because the reflection of infrared radiation is angle-dependent, while in perfectly diffuse surfaces this reflected radiation is isotropic and it is spread homogeneously in all directions. For specular targets, some valuable studies were carried out by several researchers in the last decades. Argiriou et al. [7] measured the brightness concentration distribution in the focal plane of a solar parabolic dish using a standard infrared thermography equipment. Bazilian et al. [8] used thermographic techniques to investigate the thermal effects of a residential-scale building integrated photovoltaic cogeneration system. More recently, Pfänder et al. [9] developed a methodology for infrared temperature measurements on solar trough absorber tubes by using a solar-blind approach. Datcu et al. [10] present a method to quantify the reflected flux of opaque walls by using an infrared mirror, which allows large surface temperature measurements by infrared thermography under near-ambient conditions with improved accuracy. Krenzinger and De Andrade [11] studied the errors and their consequences when performing outdoor glass thermographic thermometry of solar energy devices. They proposed and experimentally validated a correction method for outdoor thermographic measurements that includes the estimation of a thermographic equivalent sky temperature. The authors applied the methodology to measurements of photovoltaic modules exposed to clear and cloudy skies. The present paper is based on the Krenzinger and De Andrade [11] research, and it extend their results to other surfaces as metallic ones, providing also a method to estimate the optimum source temperature and the analysis of the measurement error.

Thermographic measurement of specular surfaces is not straightforward. Specular reflection is mirrorlike, that is, the incident angle is equal to the reflected angle with both angles and the normal to surface lying on the same plane. Thus, the contribution of the reflected energy to the thermal image produced by a thermographic camera is an important parameter that should be accounted for. Pfänder et al. [9] highlights two main limitations for the accurate temperature determination when using infrared sensors on solar irradiated surfaces: reflected infrared energy from sunlight and errors due to the uncertainty in the emittance of the radiating object. The authors studied the application of thermography in the tubes of a solar absorber and they indicate that reflection errors are often dominant for measurements under concentrated solar radiation and that a reliable temperature measurement is only possible if the thermal radiance considerably exceeds the reflected radiance. When this is not the case, as for example when glazed surface at near ambient temperature are inspected, the knowledge of infrared reflectance is important for the analysis and processing of the thermal image. Thus, in quantitative applications of thermography, the estimation of the infrared reflectance provides vital information in order to correct the measurements provided by the camera. It is also important for specular materials to know the behavior of the reflectance with the incidence angle in order to correct the measurements that were taken with incidence angles different from the normal direction, and for surfaces that are not plane.

This work describes a methodology to measure the reflectance of specular materials for different incidence angles in the infrared range 8 μm–14 μm, by using a thermographic camera and an infrared radiation source. The methodology includes the analysis of errors in the estimation of the reflectance and how to select the temperature of the source that minimizes these errors. The method is applied to different specular surfaces commonly used in building facades and solar devices, whose infrared specular reflectances are estimated for different incidence angles. The obtained results are analyzed in order to provide valuable information for in-situ thermographic measurements of specular surfaces.

2. Reflectance of specular surfaces

In specular reflection, a monochromatic parallel beam from a single incoming direction $i_{\lambda,i}(\lambda,\theta,\varphi)$ is reflected into a single outgoing direction, where the angle of incidence of the incoming ray θ equals the angle of reflection θ_r and that the incident, normal to surface and reflected directions are coplanar. The reflectance of a surface is defined as the ratio of reflected power to incident power incoming, that is, for a monochromatic beam of wavelength λ the reflectance at an incidence angle θ and azimuth φ is defined as:

$$\rho_\lambda(\theta,\phi) = i_{\lambda,r}(\lambda,\theta_r = \theta,\phi_r = \phi+\pi)/i_{\lambda,i}(\lambda,\theta,\varphi) \quad (1)$$

In real surfaces, there is not a single outgoing direction of the reflected ray, but a narrow cone, due to the surface roughness. Expressions relating the roughness of a plane surface to its specular reflectance at normal incidence were presented and were experimentally in the early '60 by Bennett and Porteus [12]. The authors stated that, if light of a sufficiently long wavelength is used, the decrease in measured specular reflectance due to surface roughness is a function only of the root mean square height of the surface irregularities, and in this cases the measurement of long-wavelength specular reflectance provide a simple and sensitive method for accurate measurement of surface finish.

Nowadays, measurements of specular reflection are performed with normal or varying incidence reflectometers using a scanning variable-wavelength light source. Fig. 1 shows the spectral reflectance at normal incidence of a glass sheet for wavelengths in the range between 0.2 and 15 μm [14]. As shown, reflectance is constant around 0.07 for the visible range (0.38–0.78 μm) and at wavelengths lower than 8 μm. Fort the range from 8 μm to 15 μm the reflectance oscillates between 0.07 and 0.25, with a maximum of 0.25 around 10 μm. Fig. 1 shows that glass is opaque to infrared radiation of wavelength greater than 5 μm, thus reflection occurs in a single interface (air) and the relationship ρ_t versus λ will be the same for a glass sheet that one cover or several glass covers. Because glass infrared transmittance is null, then the incident radiation must be absorbed or reflected. This behavior is different in the visible range, where transmittance is high and it decreases with the incidence angle (Duffie and Beckman [13]).

Usually the values of reflectance are done for a specific range of interest λ_1–λ_2. In this case, the specular reflectance given by the previous equation is integrated over the corresponding range as shown in Eq. (2).

$$\rho_{\lambda_1-\lambda_2} = \frac{\int_{\lambda_1}^{\lambda_2} i_{\lambda,r}(\lambda,\theta_r = \theta,\phi_r = \phi+\pi)d\lambda}{\int_{\lambda_1}^{\lambda_2} i_{\lambda,i}(\lambda,\theta,\phi)d\lambda} \quad (2)$$

The reflectance is named visible, infrared or solar, according to the range λ_1–λ_2 considered as the integration limits, and these values are usually found in the bibliography at normal incidence. In the case of the thermographic cameras, the common ranges are 8–14 μm or 2–5.6 μm, due to low atmosphere absorption in both ranges. In our particular case, the range of the camera is 8–14 μm, thus in the following paragraphs we will name ρ_t to the target specular infrared reflectance in the range 8–14 μm, at an incidence angle θ and at an azimuthal angle φ.

3. Infrared radiometric thermometry

As explained before, a thermographic camera detects the radiant energy over a range of wavelengths (usually 8–14 μm or 2–5.6 μm) emitted by the object of interest, and by using Planck's radiation law it relates this energy to the object temperature and transforms the radiometric measure into a visible color or gray image. The sensor technology is an array of uncooled microbolometers of vanadium oxide (VOx) or amorphous silicon (a-Si) with a large temperature coefficient on a silicon element with large surface area, low heat capacity and good thermal insulation [15,16], that produces an electrical signal S_{sen} proportional to the absorbed radiation.

For opaque targets placed in an ambient with low humidity and surrounding temperature near air temperature, S_{sen} is expressed as (Gaussorges [17]):

$$S_{sen} = \varepsilon_t S_0(T_t) + (1-\varepsilon_t)S_0(T_a) \quad (3)$$

where $S_0(T)$ is the signal produced by a sensor (V) when infrared radiation exclusively from a blackbody at temperature T arrives it, ε_t is the target effective emittance, T_a is the air temperature (°C) and T_t the target temperature (°C).

The relationship between $S_0(T)$ and T is a characteristic of the sensor and camera optics, and it is usually unavailable to the user. When the user sets the values of ε_t and T_a, the camera is able to calculate T_t by using Eq. (3) and the sensed electrical signal S_{sen}. The results are stored in a radiometric data file which is not directly accessible to the user and a manufacturer's own soft provided with the camera must be used. Because the files are radiometric, there is

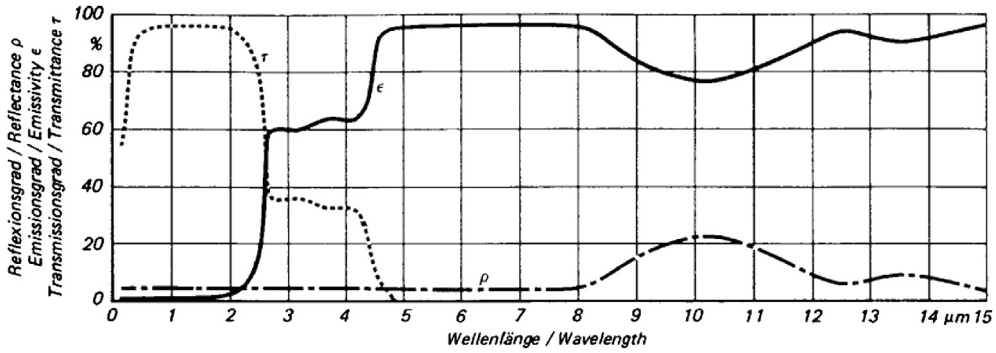

Fig. 1. Spectral reflectance of a glass sheet. Source: VDI/VDE Richtlinie, 1995 [14].

not necessary to define the setting values in the instant of the measurement but later, when processing the results in the software.

3.1. Reflectance determination

The methodology includes the inspection of two opaque bodies: an infrared source of emittance ε_s at temperature T_s and a specular target of emittance ε_t and reflectance ρ_t at ambient air temperature T_a. When the infrared source is measured, the signal $S_{sen,s}$ detected by the sensors includes the two terms given by Eq. (3):

$$S_{sen,s} = \varepsilon_s S_0(T_s) + (1-\varepsilon_s) S_0(T_a) \tag{4}$$

To ensure the specular target is at ambient temperature T_a, the measurement of the reflected image must be taken so quickly as to avoid the heating of the target surface due to absorption of the radiation emitted by the infrared source (if the target is heated up, then it will be necessary to know the camera response, which is not available to the end-user, to compute the target reflectance). Thus, when the image of the source reflected by the target surface is inspected, the signal $S_{sen,r}$ includes the radiation emitted by the target at temperature T_a and the radiation coming from the source that is specularly reflected by the target:

$$S_{sen,r} = \varepsilon_t S_0(T_a) + \rho_t S_{sen,s} \tag{5}$$

In the case of diffusing surfaces, a portion of the radiation arriving the target is reflected in all directions and do not reach the camera sensors. In the case of a perfectly diffusing opaque target, Eq. (5) must be corrected in order to include the view factors between the source, the target and the camera lenses. The extension of the method for diffusing surfaces will be faced in future studies.

Fig. 2 shows a scheme for the radiation arriving the sensor after it was reflected by the specular target. The signal $S_{sen,r}$ is processed by the camera software. When the emissivity is setted to ε', the fictitious or apparent temperature of the reflection T_r is calculated by the software as:

$$S_{sen,r} = \varepsilon' S_0(T_r) + (1-\varepsilon') S_0(T_a) \tag{6}$$

Equaling Eqs. (5) and (6) and selecting an emittance $\varepsilon' = \varepsilon_s$ when processing the reflected apparent temperature, we obtain:

$$\rho_t = \frac{S_0(T_r) - S_0(T_a)}{S_0(T_s) - S_0(T_a)} \tag{7}$$

Eq. (7) shows that to calculate ρ_t it is not necessary to know the exact value of ε_s provided that both, the source and the reflected temperatures, were taken with the same setted emittance value.

To evaluate the expression (7), we need to know $S_0(T)$. Many expressions exists in the bibliography that represents the response of infrared sensors, the most known and used being those proposed by Sakuma and Hattori [18] and by Sakuma and Kobayashi [19]. We selected the potential expression $S_0(T) = CT^A$ where C is a constant and $A = 4$, because this equation allows the results to be analyzed through an expression similar to the Stefan Boltzmann law, and because it is one of the most utilized expressions in the bibliography. Thus, the reflectance ρ_t is determined as:

$$\rho_t = \frac{(T_r+273)^4 - (T_a+273)^4}{(T_s+273)^4 - (T_a+273)^4} \tag{8}$$

where T_s is the temperature (°C) of the source measured by the camera T_a, is the air temperature (°C), and T_r is the apparent reflected temperature (°C) when the set emittances of all measurements to the same value. This reflectance can be determined for different incidence angles of the beam incoming radiation.

3.2. Error analysis

To analyze the error of the reflectance measurement, we need to include the equipment errors in the sensed temperatures, that is, the absolute errors ΔT_s, ΔT_r and ΔT_a in determining the source, reflected and air temperatures. The absolute error in the reflectance $\Delta\rho_t$ is found by the propagation method in Eq. (8) (Taylor [20]):

$$\Delta\rho_t = \sqrt{\left(\Delta T_s \frac{\partial \rho_t}{\partial T_s}\Big|_{T_r,T_a}\right)^2 + \left(\Delta T_r \frac{\partial \rho_t}{\partial T_r}\Big|_{T_s,T_a}\right)^2 + \left(\Delta T_a \frac{\partial \rho_t}{\partial T_a}\Big|_{T_r,T_s}\right)^2} \tag{9}$$

while the percentage error $e\%$ is calculated as the ratio in percent between the absolute error and the measured value.

Once the equipment was selected, the only variable that can be modified by the user that influences the relative error is the source temperature T_s. The dependence of $e\%$ with T_s was calculated for $T_a = 20.0$ °C and it is presented in Fig. 3 for different reflectances between 0.1 and 0.8. The absolute error of the air temperature was ±0.4 °C (corresponding to a digital thermometer with a K-thermocouple). ΔT_s and ΔT_r were determined by using the error specified by the manufacturer of the thermographic camera (±2 °C or ±2% *of the measured value*, whichever is greater). Fig. 3 shows that the minimum achievable error is around 5% and that $e\%$ decreases when ρ_t increases. Also it can be concluded that for materials with low reflectances (glazed surfaces) there are more adequate higher source temperatures. For these materials, errors can be as high as 44% for source temperatures of around 60 °C. In the case of surfaces with high reflectances (generally metallic ones) the selection of the source temperature is less influencing than for glass: it varies from

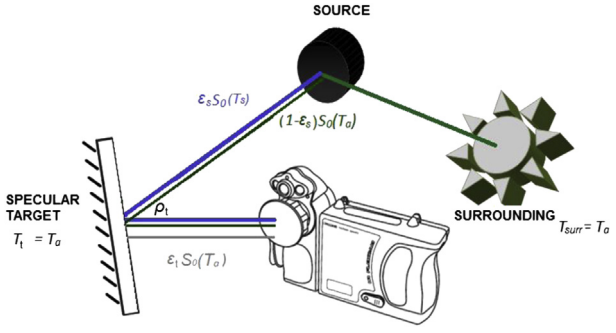

Fig. 2. Scheme of the radiation arriving the camera after the reflection in the specular surface of the target.

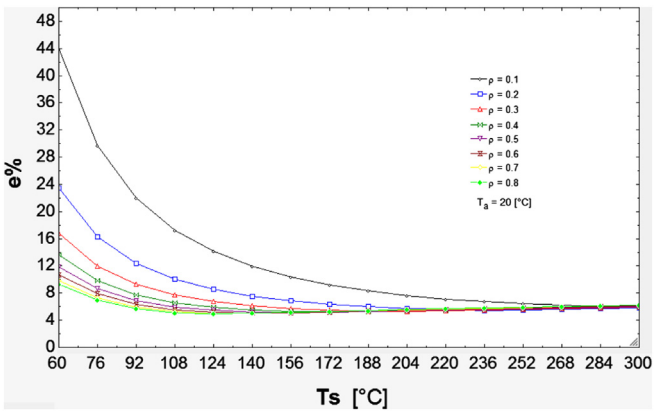

Fig. 3. $e\%$ in function of T_s for different ρ_t values, at an air temperature of 20 °C.

9% to 4%. For example, for a source temperature of 100 °C, *e*% is around 14% for a glass target ($\rho_t \sim 0.15$) and around 5% for a metallic target ($\rho_t \sim 0.8$). The curves of Fig. 3 also show that, depending on the material reflectance, there is a source temperature for which the relative error is minimum. This value should be considered together with the camera and source ranges in order to select the most appropriate source temperature without affecting the source temperature stability.

In order to assess the optimum values of the source temperature for a given material, the derivative of the relative error with respect to T_s was equaled to zero and the source temperature was found from the resulting equation. The calculation was made through the computational software EES (Engineering Equation Solver) and the results of $T_{s,min} = f(\rho_t)$ are presented in Fig. 4, for three air temperature conditions (15 °C, 20 °C and 25 °C). The horizontal bars on each point indicate the error band of the measurement. Due to the proximity of the curves only the error bars for $T_a = 20$ °C are shown. The influence of the air temperature on the relative error was also calculated and it was found to be lower than 0.25%, so it is not necessary to reduce the air temperature of the laboratory for tests.

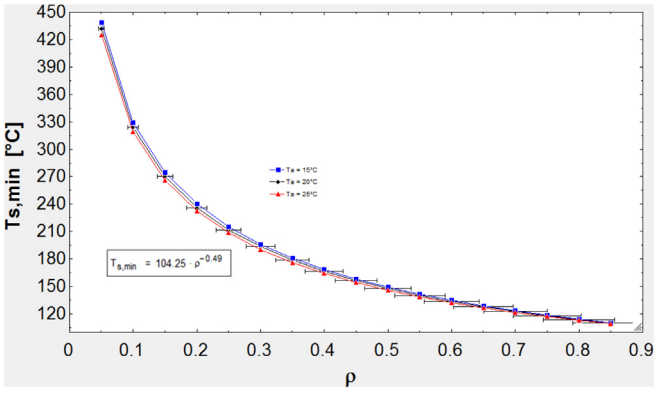

Fig. 4. $T_{s,min}$ vs ρ_t, for different air temperatures $T_a = 15$ °C, $T_a = 20$ °C and $T_a = 25$ °C.

4. Experimental layout

4.1. Methodology

The experimental layout consists of a specular target placed at vertical position and both source and camera placed equidistant to the normal of the target surface, as shown in Fig. 5 for an incidence angle of $\theta = 45°$. The methodology consists in taking two thermographic images, one of the infrared radiation source and the other of its reflection on the specular surface. The process is repeated for each incidence angle. Finally, the temperatures T_r and T_s are extracted from the thermograms by using the software provided with the camera, and Eqs. (8) and (9) are used to obtain the specular reflectance and its corresponding error.

The first decision to make is to select the kind of infrared source to use and its temperature. It is preferable an extended source than a punctual one because thermograms of an extended area allow the determination of the source temperature with a higher precision. Software of digital image processing can be used, for example to obtain averaged values, maxima and minima values, temperature profiles, etc. While the more uniform the temperature distribution of the source surface, the higher the measurement quality of the source temperature. The second aspect to be considered is the selection of the source temperature. As explained in the previous section, it depends on the target surface. For example, in the case of glass and mirrors, infrared reflectance is around 0.15 and the optimum source temperature for at $T_a = 20$ °C is around 270 °C, while

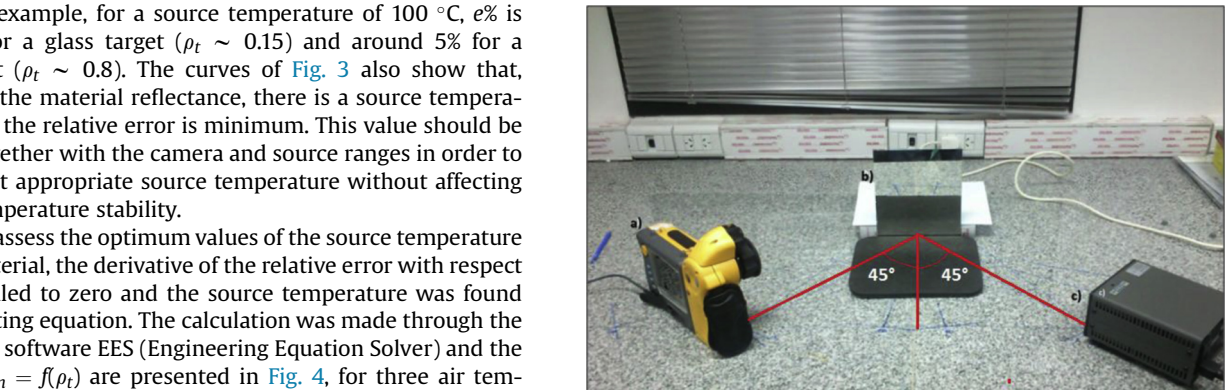

Fig. 5. Experimental layout. (a) Thermographic camera, (b) specular target, and (c) infrared radiation source, positioned to make measurements for $\theta = 45°$.

in metals the infrared reflectance is around 0.8 and the optimum source temperature is around 110 °C.

The environment of the target must be maintained as constant as possible: air temperature should be constant and known, with negligible air flows to avoid convective heat losses of the measured surfaces, and external radiation sources (as computers, lights, air heaters, etc.) should be eliminated by turning them off. Fig. 6 shows the two thermographic images, one of the infrared radiation source and the other of its reflection on the specular surface. Note the specularity in the infrared range: the reflected image is not distorted. In order to avoid the heating of the surface sample, the thermographic images are taken in a few seconds.

4.2. Equipment description

The infrared radiation source is an IR calibrator Hart Scientific model 9132. It has a diffuse black circular surface (diameter 57 mm) of known emittance ($\varepsilon_s = 0.95$). The disk can be heated uniformly to a constant temperature selected by the user in the range 50 °C–500 °C. A stabilization time of around 30 min is required in order to ensure the set temperature was reached. The set temperature was 90 °C for all samples, that is, from Fig. 3 percentage errors were around 6% (for metals) and 16% (for glass). The selection was made by considering that lower source temperatures are more stable than higher ones, that the mentioned error range is quite good for the measurements, and that a blackbody at 90 °C has its maximum emission in the detection range of the camera sensors. The temperature of the air in the laboratory was maintained at constant temperature by a split-type air conditioning equipment with thermostat. The air temperature was measured with a digital thermometer FLUKE 54II, with an accuracy of 0.05% *of measured value* +0.3 °C. Air temperature was 20.0 °C ± 0.4 °C. Doors and windows were closed to prevent air flows, and there were not external radiation sources.

The thermographic camera is a FLUKE Ti55 camera with fusion of visible and thermal images. It works in three temperature ranges: −20 °C–100 °C, −20 °C–350 °C, and 250 °C–600 °C, with an accuracy of 2% or 2 °C (whichever is greater). The image sizes are 320 × 240 in the IR range and 1280 × 1024 in the visible range. The analysis of the thermograms was made through SmartView software that was provided with the camera. The camera settings were: range −20 °C to 100 °C, background temperature $T_a = 20$ °C, air transmittance $\tau_a = 1$ and emittance is set to 0.95.

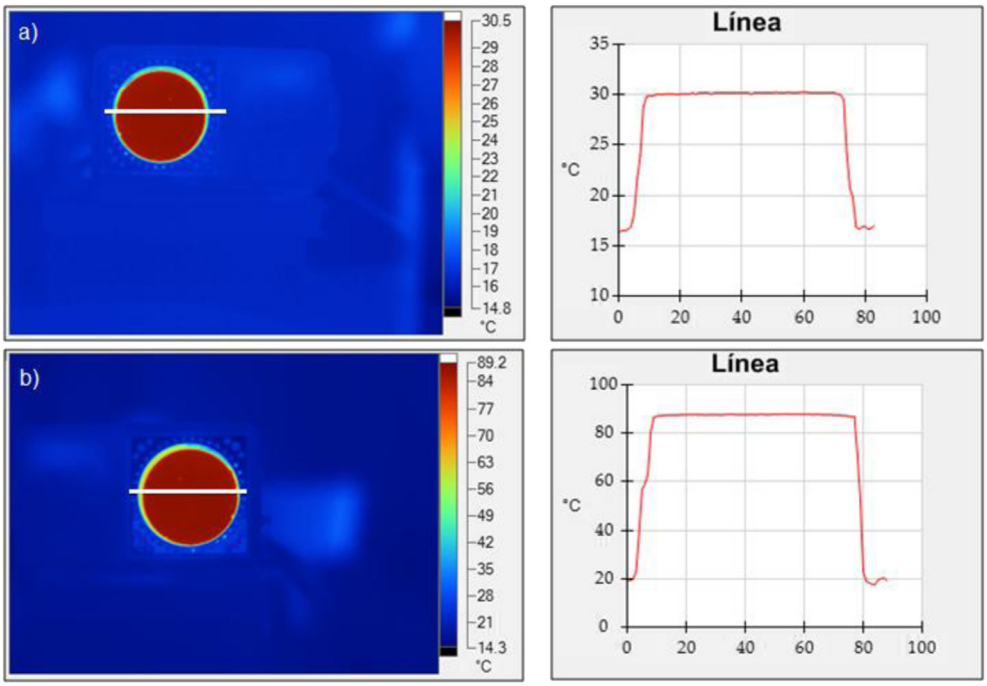

Fig. 6. a) Infrared reflected image and temperature profile on the gray line produced by a mirror target and b) infrared image of the source set to 90 °C. $\theta = 45°$. Scales of both images are different.

The materials tested were:

* Mirrors of different thicknesses and qualities: 3 mm and 4 mm thick mirrors with common glass support, and 4 mm thick mirror with "white" glass support (low iron content).
* Glass of different thicknesses: 2 mm and 8 mm thick common clear glass.
* Aluminum sheet (Al 98.8%), with one anodized and polished face and other anodized and unpolished face. Both faces were measured.

All surfaces are cleaned with alcohol before the measurements. The image of the source reflected on the aluminum sheet was slightly different of a perfect circle, thus evidencing that the aluminum sheet is not perfectly plane. This situation can introduce errors of at least 0.5 °C in the registered temperatures resulting in variations of the reflectance of around 1%.

4.3. Results

Fig. 7 shows the reflectance obtained for the targets at incidence angles between 10° and 70°, with the error bars calculated through Eq. (9). Two fitting curves with their mathematical expressions were included in the graphic, both with R^2 around 0.97. As expected, a very different behavior is observed between the group of metal surfaces and the group of glass surfaces: for materials with glass as substrate the specular reflectance ρ_t increases with the incidence angle θ, while for the metal sheet ρ_t decreases when θ increases.

In the case of glazed substrates, reflectance is almost the same for all samples: mirrors and glasses of different thicknesses and iron content present similar values of ρ_t, with small differences below 5%. From this group, the mirror target with 4 mm "white" glass support presents the greatest reflectances for all angles. The reflectance is constant below $\theta = 45°$, taking a mean value of $\rho_t = 0.15 \pm 0.03$ for all targets. This value is close to the ones given in the literature: Raytek [21] reports a reflectance at normal incidence of 0.15 ($\varepsilon = 0.85$) for glass surfaces in the range 8–14 μm, while Krenzinger and De Andrade [11] report the same value in this wavelength band. When the incidence angle is increased behind 45° the reflectance grows up, reaching a maximum value of 0.52 for an angle of 80°. Other researchers have found the same growing behavior, but with a slightly lower slope [11] that gives a maximum value of 0.43 for an angle of 80° with a maximum error of around 0.05. The differences can arise from the glass composition: the iron content in the form of iron salts impairs the radiation transmission, thus influencing the optical glass refraction index and hence the reflectance. The variation of ρ, and consequently the emittance, with the incidence angle suggests that thermograms should be taken at small incidence angles if literature values are used to set the camera. When the view angle is higher than 45°, the emittance value must be set correctly in the camera software in order to avoid erroneous temperature

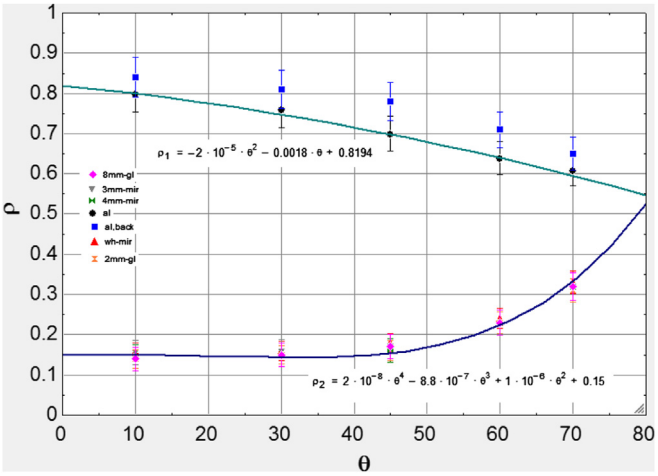

Fig. 7. Specular reflectance ρ_t vs incidence angle θ results for all samples with their corresponding error bars.

estimation. This could be the case of thermograms of high-rise glazed building facades taken from the street level.

In the case of metal sheets, Fig. 7 shows that the polished side presents ρ_t values between 0.82 and 0.55 with an average absolute error of ±0.05. The normal incidence value agree with the manufacturer value, that reports an infrared reflectance of 0.8 ($\varepsilon = 0.2 \pm 0.03$ at 100 °C) [22]. Other values found in the literature varies from 0.7 to 0.9 in the range 8–14 μm for polished surface and up to 0.95 for special aluminum sheets applied in solar devices [22,23]. Fig. 7 shows that the behavior of the reflectance with the incidence angle is opposite to that of glass: it decreases with increasing incidence angles and there is not an angle band where the reflectance remains constant. This means that care must be taken when measuring metallic surfaces: both, the incidence angle must be known, and the thermal emittance at this angle must be correctly set. No literature was found that addresses this behavior.

Finally, Fig. 7 shows that the specular reflectance of the unpolished back side presents values from 0.87 to 0.60, values that are 6–8% higher than those of the polished surface. The difference arise from the surface back side treatment: the unpolished surface is less specular than the front polished one, so a portion of radiation is specularly reflected and a portion is diffusely reflected, thus the area seen by the sensor could contain a small additional contribution of adjacent points that increase ρ_t values. As explained before, the developed method can be applied only for specular surfaces.

5. Conclusions

A simple methodology to estimate the reflectance of specular materials for different incidence angles in the infrared range 8 μm–14 μm, by using a thermographic camera and an infrared radiation source, was developed. The methodology consists in taking two thermographic images, one of an infrared radiation source and the other of its reflection on the specular surface, and by using Eqs. (8) and (9) the specular reflectance and its corresponding error are obtained. An important conclusion is that the source temperature influences the error of the measurement, especially for glass targets, and graphs are included to select the temperature of the source that minimizes the measurement error. This methodology can be applied to determine the infrared behavior of different kind of special glasses available in the market, as low-e and selective glasses, and for surfaces of solar devices as glazed covers of solar air and water collectors, solar absorbers, etc.

The methodology was applied to different specular surfaces commonly used in building facades and solar devices: mirrors of different thicknesses and qualities (3 mm and 4 mm thick mirrors with common glass support, 4 mm thick mirror with “white” glass support, 2 mm and 8 mm thick common clear glass), and a metal aluminum sheet (with one anodized and polished face and other anodized and unpolished face). The infrared specular reflectances were estimated for different incidence angles and fitting equations were provided. In the case of glass and mirrors, the measurements show that for incidence angles below 45°, both reflectance and emittance presents low variations, but for incidence angle higher than 45°, reflectance is higher and emittance ($\varepsilon_t = 1 - \rho_t$) must be set correctly in the camera software in order to avoid an erroneous temperature estimation. This could be the case of thermograms of high-rise glazed building facades taken from the street level. The measured mean reflectance below $\theta = 45°$ is $\rho_t = 0.15 \pm 0.03$ and it is constant for incidence angles between 0° and 45°. For incidence angles higher than 45° the reflectance grows up to 0.52 and the reflectance can be estimated through the provided fitting equation.

In the case of the metal aluminum sheet, reflectance values of the unpolished side are between 6 and 8% higher than those of the polished one that can be explained by contributions other than specular due to the lesser specularity of the unpolished side. The measurements on the polished side showed reflectance values carrying between 0.82 and 0.55, with average absolute errors of ±0.05. The values obtained in the measurements are similar to those reported by the bibliography, ensuring the adequacy and accuracy of the methodology.

Because in metallic surfaces the infrared reflectance is highly variable in the whole measurement range 10°–70°, care must be taken when measuring metallic surfaces: both, the incidence angle must be known, and the thermal emittance at this angle must be correctly set in the camera.

Special caution is needed when the target surface is not specular. In the case of diffusing opaque surfaces, a portion of the radiation arriving the target is reflected in all directions and do not reach the camera sensors. Thus, the methodology is not adequate and it has to be reformulated to include the view factors between the source, the target and the camera lenses. A methodology for diffuse ones will be pointed out in future works.

Acknowledgments

This research was supported by CIUNSa, Universidad Nacional de Salta, and by ANPCYT PICTO ENARGAS 2009.

References

[1] Albatici R, Tonelli A. Infrared thermovision technique for the assessment of thermal transmittance value of opaque building elements on site. Energy and Buildings 2009;42:2177–83.
[2] Chudnovsky A, Ben-Dor E, Saaroni H. Diurnal thermal behavior of selected urban objects using remote sensing measurements. Energy and Buildings 2004;36:1063–74.
[3] Asdrubali F, Baldinelli G, Bianchi F. A quantitative methodology to evaluate thermal bridges in buildings. Applied Energy 2012;97:365–73.
[4] Fokaides PA, Kalogirou SA. Application of infrared thermography for the determination of the overall heat transfer coefficient (U-Value) in building envelopes. Applied Energy 2011;88:4358–65.
[5] Lehmann B, Ghazi Wakili K, Frank Th, Vera Collado B, Tanner Ch. Effects of individual climatic parameters on the infrared thermography of buildings. Applied Energy 2013;110:29–43.
[6] Marinetti S, Cesaratto PG. Emissivity estimation for accurate quantitative thermography. NDT &E International 2012;51:127–34.
[7] Argiriou A, Papini F, Pasquetti R, Arconada A, Gallet P, Audibert M. Measurement of brightness concentration distribution in the focal zone of a focusing solar collector with an infrared camera. Solar Energy 1988;41(3):267–71.
[8] Bazilian MD, Kamalanathan H, Prasad DK. Thermographic analysis of a building integrated photovoltaic system. Renewable Energy 2002;26:449–61.
[9] Pfänder M, Lüpfert E, Pistor P. Infrared temperature measurements on solar trough absorber tubes. Solar Energy 2007;81:629–35.
[10] Datcu S, Ibos L, Candau Y, Mattei S. Improvement of building wall surface temperature measurements by infrared thermography. Infrared Physics & Technology 2005;46:451–67.
[11] Krenzinger A, de Andrade AC. Accurate outdoor glass thermographic thermometry applied to solar energy devices. Solar Energy 2007;81:1025–34.
[12] Bennet HE, Porteus JO. Relation between surface roughness and specular reflectance at normal incidence. Journal of the Optical Society of America 1961;51(2):123–9.
[13] Duffie JA, Beckman WA. Solar engineering of thermal processes. 3rd ed. New Jersey: John Wiley and Sons; 2006.
[14] VDI/VDE Richtlinie. Technische Temperaturmessungen-Strahlungs thermometrie. VDI 3511; 1995. p. 4.
[15] Rogalski A. Recent progress in infrared detector technologies. Infrared Physics & Technology 2011;54:136–54.
[16] FLIR Commercial Vision Systems B.V. Uncooled detectors for thermal imaging cameras. http://www.flirmedia.com/MMC/CVS/Appl_Stories/AS_0015_EN.pdf; 2011 [last accessed 18.02.13].
[17] Gaussorgues G. La thermographie infrarouge. 3rd ed. Paris: Technique et Documentation, Lavoiser; 1981.
[18] Sakuma F, Hattori S. Establishing a practical temperature standard by using a narrow-band radiation thermometer with a silicon detector. In: Schooley JF,

editor. Temperature: its measurement and control in science and industry, vol. 5. New York: AIP; 1982. p. 421–7.
[19] Sakuma F, Kobayashi M. Interpolation equations of scales of radiation thermometers. In: Proceedings of TEMPMEKO 1996; 1996. p. 305–10.
[20] Taylor JR. An introduction to error analysis. 2nd ed. California: University Science Books; 1997.
[21] Raytek. http://www.raytek.com/Raytek/en-r0/IREducation/EmissivityNonMetals.htm. [accessed 07.08.13].
[22] Alanod. http://alanod-solar.com/opencms/opencms/Absorption/Technische_Info.html. [accessed 07.08.13].
[23] Raytek. http://www.raytek.com/Raytek/en-r0/IREducation/EmissivityTableMetals.htm. [accessed 07.08.13].